Aging to Equilibrium Dynamics of SiO_2

K. Vollmayr-Lee* and J. A. Roman
Department of Physics and Astronomy, Bucknell University, Lewisburg, Pennsylvania 17837, USA

J. Horbach
Institut für Materialphysik im Weltraum, Deutsches Zentrum für Luft- und Raumfahrt (DLR), Linder Höhe, 51147 Köln, Germany

(Dated: May 3, 2010)

Molecular dynamics computer simulations are used to study the aging dynamics of SiO_2 (modeled by the BKS model). Starting from fully equilibrated configurations at high temperatures $T_\mathrm{i} \in \{5000\,\mathrm{K}, 3760\,\mathrm{K}\}$, the system is quenched to lower temperatures $T_\mathrm{f} \in \{2500\,\mathrm{K}, 2750\,\mathrm{K}, 3000\,\mathrm{K}, 3250\,\mathrm{K}\}$ and observed after a waiting time t_w. Since the simulation runs are long enough to reach equilibrium at T_f, we are able to study the transition from out-of-equilibrium to equilibrium dynamics. We present results for the partial structure factors, for the generalized incoherent intermediate scattering function $C_q(t_\mathrm{w}, t_\mathrm{w}+t)$, and for the mean square displacement $\Delta r^2(t_\mathrm{w}, t_\mathrm{w}+t)$. We conclude that there are three different t_w regions: (I) At very short waiting times, $C_q(t_\mathrm{w}, t_\mathrm{w}+t)$ decays very fast without forming a plateau. Similarly $\Delta r^2(t_\mathrm{w}, t_\mathrm{w}+t)$ increases without forming a plateau. (II) With increasing t_w a plateau develops in $C_q(t_\mathrm{w}, t_\mathrm{w}+t)$ and $\Delta r^2(t_\mathrm{w}, t_\mathrm{w}+t)$. For intermediate waiting times the plateau height is independent of t_w and T_i. Time superposition applies, i.e. $C_q = C_q(t/t_\mathrm{r}^\mathrm{Cq})$ where $t_\mathrm{r}^\mathrm{Cq} = t_\mathrm{r}^\mathrm{Cq}(t_\mathrm{w})$ is a waiting time dependent decay time. Furthermore $C_q = C(q, t_\mathrm{w}, t_\mathrm{w}+t)$ scales as $C_q = C(q, z(t_\mathrm{w}, t)$ where z is a function of t_w and t only, i.e. independent of q. (III) At large t_w the system reaches equilibrium, i.e. $C_q(t_\mathrm{w}, t_\mathrm{w}+t)$ and $\Delta r^2(t_\mathrm{w}, t_\mathrm{w}+t)$ are independent of t_w and T_i. For $C_q(t_\mathrm{w}, t_\mathrm{w}+t)$ we find that the time superposition of intermediate waiting times (II) includes the equilibrium curve (III).

PACS numbers: 61.20.Lc, 61.20.Ja, 64.70.ph, 02.70.Ns, 61.43.Fs

I. INTRODUCTION

When a glass-forming liquid is quenched from an equilibrium state at a high temperature T_i to a non-equilibrium state at a lower temperature T_f, "aging processes" set in. Provided that crystallization plays no role at T_f (e.g. due to very low crystal nucleation rates), the transition to a final (metastable) equilibrium state occurs on a time scale that corresponds to the typical equilibrium relaxation time τ_eq of the (supercooled) liquid at T_f. The dynamics of the system depends on the waiting time t_w which is the time elapsed after the temperature quench. If τ_eq exceeds the waiting time t_w then the system is observed in a transient non-equilibrium state which corresponds to a glass for $t_\mathrm{w} \ll \tau_\mathrm{eq}$. During the aging process, i.e. for $t_\mathrm{w} < \tau_\mathrm{eq}$, thermodynamic properties such as volume and energy are changing and time translation invariance does not hold: correlation functions at time $t_\mathrm{w}+t$ and the time origin at t_w do depend not only on the time difference t but also on the waiting time t_w.

Recently this aging process has been investigated extensively with experiments [1–6], theoretically [7–9] and with computer simulations. For a more complete summary of previous results we refer the reader to the references [10, 11] and references therein. Computer simulation studies most similar to the work presented here are on attractive colloidal systems [12–15], on the Kob-Andersen Lennard-Jones (KALJ) mixture [16–25], and silica (SiO_2) [25–28]. In the case of silica the interpretation of the results is less clear than for the KALJ mixture; e.g. different findings [25, 27] have been reported on the violation of the fluctuation-dissipation regime during aging [7–9]. Thus, it remains open whether silica, as the prototype of a glass-forming system forming a tetrahedral network structure, exhibits a different aging dynamics than, e.g. the KALJ model, where the structure is similar to that of a closed-packed hard-sphere structure.

Recent simulation studies on amorphous silica [25–39] have widely used the BKS potential [40] to model the interactions between the atoms. Although it is a simple pair potential, it reproduces various static and dynamic properties of amorphous silica very well. For BKS silica, the self-diffusion constants D_α ($\alpha = \mathrm{Si}, \mathrm{O}$) show two different temperature regimes: At high temperatures, D_α decays according to a power law, as predicted by the mode coupling theory (MCT) of the glass transition (note, however, that also other interpretations have been assigned to this high temperature regime). At low temperature, D_α as well as the shear viscosity η exhibit an Arrhenius behavior with an activation energy of the order of 5 eV, in agreement with experiment (see [30] and references therein). The temperature at which the crossover between both regimes occurs is at $T_c \approx 3300\,\mathrm{K}$, corresponding to the critical MCT temperature of BKS silica. Previous studies of the aging dynamics of BKS silica [25–27] were performed in two steps. First, the system was fully equilibrated at a temperature $T_\mathrm{i} > T_c$. Then, the

*Electronic address: kvollmay@bucknell.edu

system was quenched to a low temperature $T_f < T_c$, followed by the production runs. Wahlen and Rieger [26] analyze time-dependent correlation functions at different waiting times t_w and Berthier [25] and Scala et al. [27] study the generalized fluctuation dissipation relation and the energy landscape [27]. All three studies [25–27] investigate the early stages of the aging dynamics, i.e. the dynamics was explored on time scales that were much smaller than the equilibrium relaxation time τ_{eq} at the temperature T_f.

In this work, we also consider quenches in BKS silica from a high temperature T_i to a low temperature T_f. Different from previous simulation studies, we aim at elucidating the full transient dynamics at T_f from the initial state at $t_w = 0$ to equilibrium. To this end, temperatures T_f are chosen such that the system can be fully equilibrated on the typical time span of the MD simulation. Note that the considered temperatures $T_f \in \{2500\,\mathrm{K}, 2750\,\mathrm{K}, 3000\,\mathrm{K}, 3250\,\mathrm{K}\}$ are below the critical MCT temperatures T_c. Thus, we have access to the full aging dynamics in the experimentally relevant Arrhenius temperature regime that we have mentioned above.

The analysis of time-dependent density correlation functions $C_q(t_w, t_w+t)$ (with q the wavenumber) and the mean square displacement $\Delta r^2(t_w, t_w + t)$ reveal three different regimes of waiting times t_w: In the case of $C_q(t_w, t_w + t)$ (and similarly for $\Delta r^2(t_w, t_w + t)$) at early t_w, a rapid decay to zero is seen, without forming a plateau at intermediate times. Then, for larger values of t_w a plateau is formed. The height of this plateau grows with waiting time and becomes more pronounced, before in the final regime the plateau height is independent of t_w and T_i. In the latter regime, time superposition holds, i.e. by scaling time with a decay time t_r^{Cq} the C_q for the different values of t_w fall onto a master curve at a given wavenumber q. This behavior is very similar to that found for the KALJ mixture. However, it is different from the behavior predicted by mean-field spin glass models and the activated dynamics scaling, as proposed by Wahlen and Rieger. Thus, these results suggest that the aging dynamics in silica, the prototype of a glass-former with a tetrahedral network structure, is very similar to that of simple glass-formers with a closed-packed hard-sphere-like structure. We find a difference between the KALJ mixture and SiO_2, however, in the parametric plot of $C'_q(C_q)$. For SiO_2 $C'_q(C_q)$ shows a data collapse for different sufficiently large t_w and thus $C_q = C(q, z(t_w, t))$ whereas this data collapse does not hold as well in the case of the KALJ mixture.

The rest of the paper is organized as follows: In the next Sec. we give the details of the BKS potential and the simulation. Then, we present the results in Sec. III, before we summarize in Sec. IV. Appendix A describes the implementation of the Nosé-Hoover thermostat used in our simulation.

II. MODEL AND DETAILS OF THE SIMULATION

The interactions between the particles are modeled by the BKS potential [40] which has been used frequently and has proven to be reliable for the study of the dynamics of amorphous silica [25–39] The functional form of the BKS potential is given by a sum of a Coulomb term, an exponential and a van der Waals term. Thus the potential between particles i and j, a distance r_{ij} apart, is given by

$$\phi(r_{ij}) = \frac{q_i q_j e^2}{r_{ij}} + A_{ij} e^{-B_{ij} r_{ij}} - \frac{C_{ij}}{r_{ij}^6} \quad , \qquad (1)$$

where e is the charge of an electron and the constants A_{ij}, B_{ij} and C_{ij} are $A_{SiSi} = 0.0\,\mathrm{eV}$, $A_{SiO} = 18003.7572\,\mathrm{eV}$, $A_{OO} = 1388.7730\,\mathrm{eV}$, $B_{SiSi} = 0.0\,\mathrm{Å}^{-1}$, $B_{SiO} = 4.87318\,\mathrm{Å}^{-1}$, $B_{OO} = 2.76000\,\mathrm{Å}^{-1}$, $C_{SiSi} = 0.0\,\mathrm{eVÅ}^{-6}$, $C_{SiO} = 133.5381\,\mathrm{eVÅ}^{-6}$ and $C_{OO} = 175.0000\,\mathrm{eVÅ}^{-6}$ [40]. The partial charges q_i are $q_{Si} = 2.4$ and $q_O = -1.2$ and e^2 is given by $1602.19/(4\pi 8.8542)\,\mathrm{eVÅ}$.

The Coulombic part of the interaction was computed by using the Ewald method [41, 42] with a constant $\alpha L = 6.3452$, where L is the size of the cubic box, and by using all q-vectors with $|q| \leq 6 \cdot 2\pi/L$. [51]. We ensure that the Ewald term in real space is also differentiable at the cutoff by smoothing similarly to Eq. (3) in [43] with $r_c = 8\,\mathrm{Å}$ and $d = 0.05\,\mathrm{Å}^2$. To increase computation speed the non-Coulombic contribution to the potential was truncated, smoothed and shifted at a distance of 5.5 Å. Note that this truncation is not negligible since it affects the pressure of the system. In Ref. [43] further slight variations on the potential are described in detail [52]. In order to minimize surface effects periodic boundary conditions were used. The masses of the Si and O atoms were 28.086 u and 15.9994 u, respectively. The number of particles was 336, of which 112 were silica atoms and 224 were oxygen atoms. For all simulation runs the size of the cubic box was fixed to $L = 16.920468\,\mathrm{Å}$ which corresponds to a density of $\rho = 2.323\,\mathrm{g/cm^3}$, a value that is very close to the one of real silica glass, $\rho = 2.2\,\mathrm{g/cm^3}$ [44].

We investigated the aging dynamics for systems which were quenched from a high temperature T_i to a low temperature T_f. To increase the statistics, for each (T_i, T_f) 20 independent simulation runs were performed. To obtain 20 independent configurations we carried out molecular dynamics (MD) simulations using the velocity Verlet algorithm with a time step of 1.6 fs at 6000 K. The temperature was kept constant at 6000 K with a stochastic heat bath by replacing the velocities of all particles by new velocities drawn from the corresponding Boltzmann distribution every 150 time steps. Independent configurations were at least 3.27 ns apart. Each of these configurations undergoes the following sequence of simulation runs (see also Fig. 1). After fully equilibrating the samples at

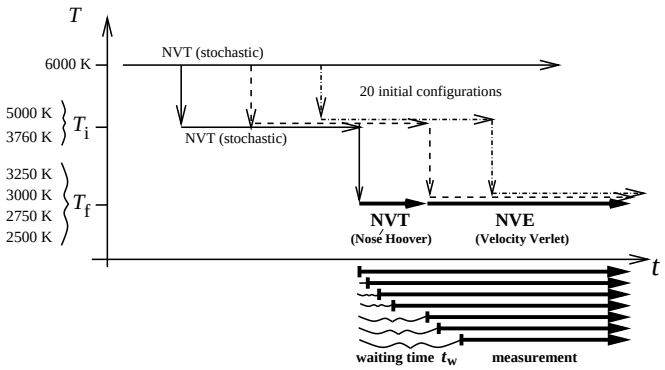

FIG. 1: Schematic sketch of the protocol for the simulation runs. 20 independent initial configurations are obtained via one long simulation run at 6000 K. For each independent configuration the system is quenched instantaneously and then fully equilibrated at temperatures $T_\mathrm{i} = 3760\,\mathrm{K}$ and 5000 K, followed by instantaneous quenches to the temperatures $T_\mathrm{f} = 3250\,\mathrm{K}$, 3000 K, 2750 K, and 2500 K. At each T_f, time-dependent correlation functions are determined for different waiting times t_w. Temperature is kept constant at T_f by coupling the system to a Nosé-Hoover thermostat. The thermostat is switched off after 0.33 ns, followed by the continuation of the simulations in the microcanonical ensemble for 33 ns.

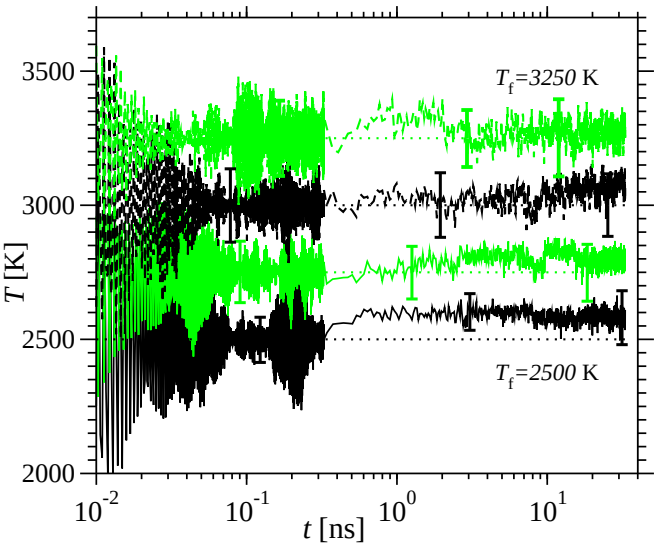

FIG. 2: (Color online) Temperature $T = \frac{2\overline{E}_\mathrm{kin}}{3N}$ as a function of time t for $T_\mathrm{i} = 5000\,\mathrm{K}$, $T_\mathrm{f} = 2500\,\mathrm{K}, 2750\,\mathrm{K}, 3000\,\mathrm{K}, 3250\,\mathrm{K}$ shown in each case for the 11th independent simulation run. $\overline{E}_\mathrm{kin}$ includes a time average and error bars indicate the corresponding fluctuations.

the initial temperatures $T_\mathrm{i} = 5000\,\mathrm{K}$ (for 16.35 ns) and $T_\mathrm{i} = 3760\,\mathrm{K}$ (for 32.7 ns), the system was quenched instantaneously to $T_\mathrm{f} \in \{2500\,\mathrm{K}, 2750\,\mathrm{K}, 3000\,\mathrm{K}, 3250\,\mathrm{K}\}$. To disturb the dynamics minimally, we used a Nosé-Hoover thermostat [45, 46] instead of a stochastic heat bath to keep the temperature at T_f constant. A velocity Verlet algorithm was used to integrate the Nosé-Hoover equations of motion (see Appendix A) with a time step of 1.02 fs. After 0.33 ns the Nosé-Hoover thermostat was switched off and the simulation was continued in the NVE ensemble for 33 ns using a time step of 1.6 fs. Whereas previous simulations used instead the NVT ensemble for the whole simulation run, we chose to switch to the NVE ensemble to minimize any influence on the dynamics due to the chosen heat bath algorithm. For the comparison with previous simulations and to check for the lack of a temperature drift, we show in Fig. 2 for exemplatory simulation runs the temperature $T = \frac{2\overline{E}_\mathrm{kin}}{3N}$ as a function of time where $\overline{E}_\mathrm{kin}$ is the time averaged kinetic energy with fluctuations as indicated with error bars. We find that even after switching off the heat bath [53] there is no temperature drift for $T = 3250\,\mathrm{K}$ and $T = 3000\,\mathrm{K}$ and for $T = 2500\,\mathrm{K}$ and $T = 2750\,\mathrm{K}$ there is only a slight temperature drift which is of the same order as the temperature fluctuations and the drift occurs only for $t \lessapprox 0.6$ ns. For all times $t \gtrapprox 0.6$ ns and for all investigated temperatures there is no temperature drift and thus the comparison with previous simulations valid.

III. RESULTS

In all following, we investigate how the structure and dynamics of the system depend on the waiting time t_w elapsed after the quench from T_i to T_f. We varied the waiting time in the range $0\,\mathrm{ns} \le t_\mathrm{w} \le 23.98\,\mathrm{ns}$.

A. Partial Structure Factor

Figure 3 shows for the temperature quench $T_\mathrm{i} = 5000$ K to $T_\mathrm{f} = 2500$ K the partial structure factors [11]

$$S_{\alpha\beta}(q, t_\mathrm{w}) = \frac{1}{N} \left\langle \sum_{i=1}^{N_\alpha} \sum_{j=1}^{N_\beta} \mathrm{e}^{i\mathbf{q}\cdot\left(\mathbf{r}_i(t_\mathrm{w}) - \mathbf{r}_j(t_\mathrm{w})\right)} \right\rangle \quad (2)$$

where $\mathbf{r}_i$ and $\mathbf{r}_j$ are the positions of particles i and j of species $\alpha, \beta = \mathrm{O}, \mathrm{Si}$. The partial structure factors for all other $(T_\mathrm{i}, T_\mathrm{f})$ combinations are very similar. Although Fig. 3 shows $S(q, t_\mathrm{w})$ for the largest investigated temperature quench, there is only a slight t_w-dependence for very short waiting times $t_\mathrm{w} \le 0.33\,\mathrm{ns}$ and almost no t_w-dependence for $t_\mathrm{w} \ge 0.33\,\mathrm{ns}$.

B. Generalized Incoherent Intermediate Scattering Function

In this section we focus on the time-dependent generalized intermediate incoherent scattering function [11]

$$C_q(t_\mathrm{w}, t_\mathrm{w} + t) = \frac{1}{N_\alpha} \left\langle \sum_{j=1}^{N_\alpha} \mathrm{e}^{i\mathbf{q}\cdot\left(\mathbf{r}_j(t_\mathrm{w}+t) - \mathbf{r}_j(t_\mathrm{w})\right)} \right\rangle \quad (3)$$

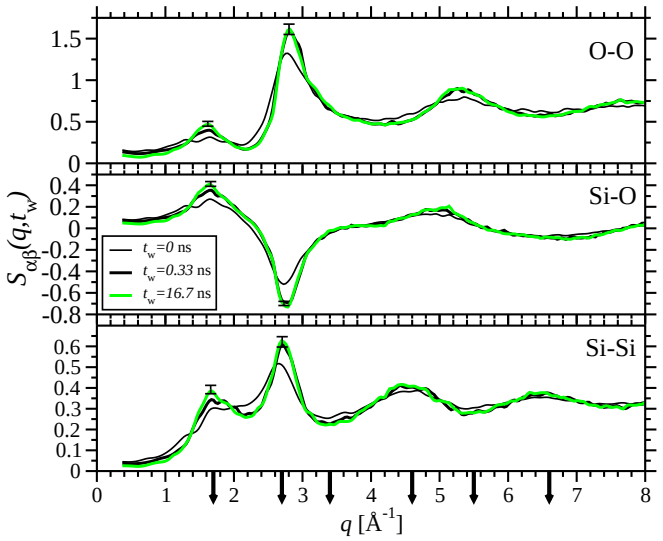

FIG. 3: (Color online) Partial structure factors $S_{\alpha\beta}(q, t_{\rm w})$ as defined in Eq. (2) for the temperature quench $T_{\rm i} = 5000\,{\rm K}$ to $T_{\rm f} = 2500\,{\rm K}$. Indicated with arrows are the wave vectors q which have been used to determine $C_q(t_{\rm w}, t_{\rm w}+t)$ as defined in Eq. (3).

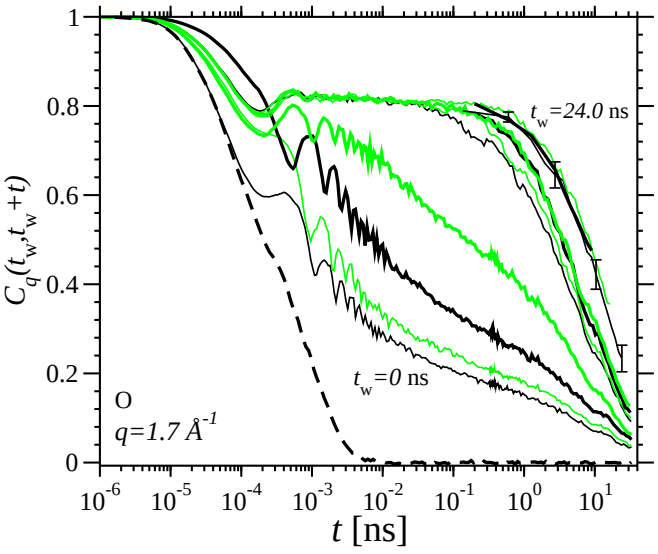

FIG. 4: (Color online) $C_q(t_{\rm w}, t_{\rm w}+t)$ as defined in Eq. (3) for the quench $T_{\rm i} = 5000\,{\rm K}$ to $T_{\rm f} = 2500\,{\rm K}$ for O-atoms and $q = 1.7\,{\rm Å}^{-1}$. Waiting times for the solid lines are from bottom to top $t_{\rm w} = 0\,{\rm ns}$, $1.63 \cdot 10^{-4}\,{\rm ns}$, $1.63 \cdot 10^{-3}\,{\rm ns}$, $1.63 \cdot 10^{-2}\,{\rm ns}$, $0.33\,{\rm ns}$, $0.49\,{\rm ns}$, $1.17\,{\rm ns}$, $1.96\,{\rm ns}$, $8.83\,{\rm ns}$, $16.67\,{\rm ns}$, and $23.98\,{\rm ns}$. The order of solid lines are for increasing $t_{\rm w}$ black thin, green (gray) thin, black thick, green (gray) thick, black thin, green (gray) thin, etc. Error bars are as indicated exemplary. The thick dashed line corresponds to $C_q(t_{\rm w}, t_{\rm w}+t) = F_{\rm s}(q,t)$ at $5000\,{\rm K}$.

which is a measure for the correlations of the positions at time $t_{\rm w}$ and at a later time $(t_{\rm w}+t)$. We investigated wave vectors of magnitude $q = 1.7, 2.7, 3.4, 4.6, 5.5$ and $6.6\,{\rm Å}^{-1}$, as indicated with arrows in Fig. 3. We show in Fig. 4 and Figs. 6 - 8 results for the first sharp diffraction peak at $q = 1.7\,{\rm Å}^{-1}$. Similar results are found for all other investigated wave vectors. Figure 4 shows $C_q(t_{\rm w}, t_{\rm w}+t)$ for the largest investigated temperature quench from $T_{\rm i} = 5000\,{\rm K}$ to $T_{\rm f} = 2500\,{\rm K}$ for waiting times $t_{\rm w} = 0$ - $23.98\,{\rm ns}$, as listed in the figure caption of Fig. 4. We find that $C_q(t_{\rm w}, t_{\rm w}+t)$ is dependent on $t_{\rm w}$ for all but the last three investigated waiting times. For very short times $t \lesssim 5 \cdot 10^{-5}$ ns and zero waiting time, $C_q(t_{\rm w}=0, t)$ is well approximated by C_q of the high temperature $T_{\rm i} = 5000$ K from which the system has been quenched (see dashed line in Fig. 4). Thus, $C_q(t_{\rm w}=0, t)$ for very short times is only dependent on $T_{\rm i}$, q and the particle type, but independent of $T_{\rm f}$. For times of the order of $t = 10^{-3}\,{\rm ns}$, $C_q(t_{\rm w}, t_{\rm w}+t)$ is oscillatory due to the small system size. For times $t \gtrsim 10^{-3}\,{\rm ns}$, C_q decays to zero without forming a plateau for small $t_{\rm w}$. With increasing $t_{\rm w}$ a plateau is formed, which is independent of t_w for $t_{\rm w} \geq 0.33\,{\rm ns}$.

To characterize the plateau height we define F as the time average of $C_q(t_{\rm w}, t_{\rm w}+t)$ for times $2.55\,{\rm ps} \leq t \leq 6.64\,{\rm ps}$. The inset of Fig. 5 shows that for large waiting times $F(t_{\rm w})$ becomes independent of $t_{\rm w}$ and of $T_{\rm i}$. To test this independence of $T_{\rm i}$ further, we show F as a function of q for $t_{\rm w} = 16.67\,{\rm ns}$ in Fig. 5. We find that the plateau height is dependent on the particle type and decreases with decreasing q, but F is independent of $T_{\rm i}$.

The plateau in C_q becomes more horizontal with decreasing final temperature $T_{\rm f}$, as can be seen by the comparison of Fig. 4 ($T_{\rm f} = 2500\,{\rm K}$) and Fig. 6 ($T_{\rm f} = 3000\,{\rm K}$). Times $t \gtrsim 0.1\,{\rm ns}$ correspond to the α-relaxation, where $C_q(t_{\rm w}, t_{\rm w}+t)$ decays from the plateau to zero. For the quench from $5000\,{\rm K}$ to $2500\,{\rm K}$ (see Fig. 4) this decay depends on $t_{\rm w}$ for all $t_{\rm w} < 8.83\,{\rm ns}$. However, for $t_{\rm w} \geq 8.83\,{\rm ns}$ (the largest three $t_{\rm w}$), $C_q(t_{\rm w}, t_{\rm w}+t)$ is independent of $t_{\rm w}$ not only for intermediate times t (plateau) but for all times (including the α-relaxation). Thus, the system reaches equilibrium during the simulation run. For the quench from $3760\,{\rm K}$ to $3000\,{\rm K}$ (see Fig. 6), $C_q(t_{\rm w}, t_{\rm w}+t)$ becomes independent of $t_{\rm w}$ for $t_{\rm w} \gtrsim 1\,{\rm ns}$, which means that the time at which equilibrium is reached is dependent on the temperature quench.

To estimate the time when the system reaches equilibrium for each $(T_{\rm i}, T_{\rm f})$ combination, we next quantify the decay of $C_q(t_{\rm w}, t_{\rm w}+t)$. Instead of taking a vertical cut in $C_q(t_{\rm w}, t_{\rm w}+t)$ as we did for F, we now take a horizontal cut. We define the decay time $t_{\rm r}^{\rm Cq}$ to be the time $t = t_{\rm r}^{\rm Cq}$ for which $C_q(t_{\rm w}, t_{\rm w}+t_{\rm r}^{\rm Cq}) = C_{\rm cut}$. We chose $C_{\rm cut} = 0.625/0.41/0.295/0.155/0.085/0.04)$ for the Si particles and $C_{\rm cut} = 0.625/0.305/0.195/0.08/0.04/0.014$ for the O particles at the wavenumbers $q = 1.7/2.7/3.4/4.6/5.5/6.6\,{\rm Å}^{-1}$, respectively. The resulting decay times $t_{\rm r}^{\rm Cq}$ as a function of waiting time $t_{\rm w}$ are shown in Fig. 7a for O-atoms and in Fig. 7b for Si-atoms. Color (black or green/gray) indicates the initial temperature $T_{\rm i}$

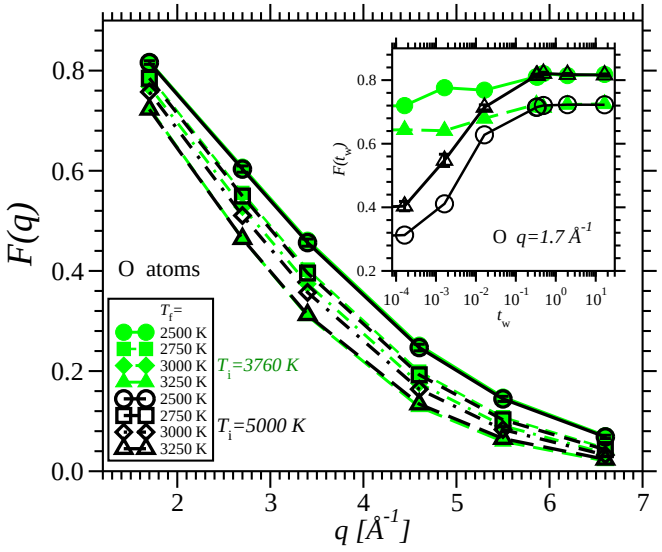

FIG. 5: (Color online) Plateau height, F, as defined in the text, as a function of wave vector q ($t_\mathrm{w} = 16.67$ ns) and in the inset as a function of t_w ($q = 1.7$ Å^{-1}). Error bars are of the same size as symbols as indicated exemplary for $T_\mathrm{i} = 5000$ K and $T_\mathrm{f} = 2500$ K.

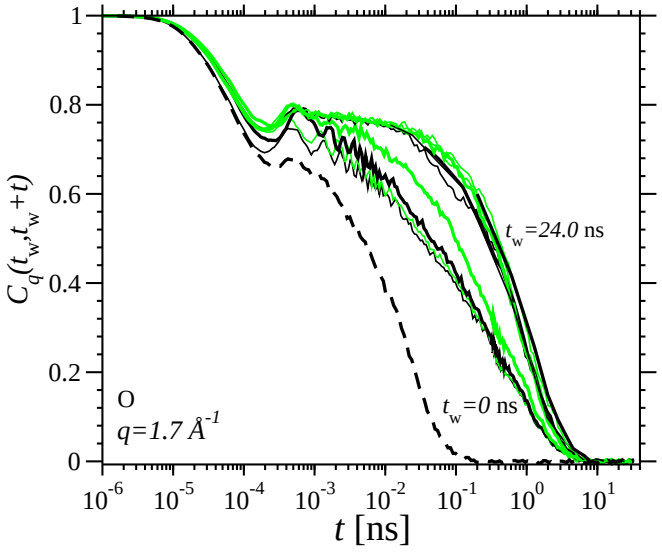

FIG. 6: (Color online) $C_q(t_\mathrm{w}, t_\mathrm{w}+t)$ for the quench $T_\mathrm{i} = 3760$ K to $T_\mathrm{f} = 3000$ K. Waiting times and corresponding line styles are the same as in Fig. 4. Error bars are of the same order as indicated in Fig. 4. The thick dashed line corresponds to $C_q(t_\mathrm{w}, t_\mathrm{w}+t) = F_\mathrm{s}(q,t)$ at 3760 K.

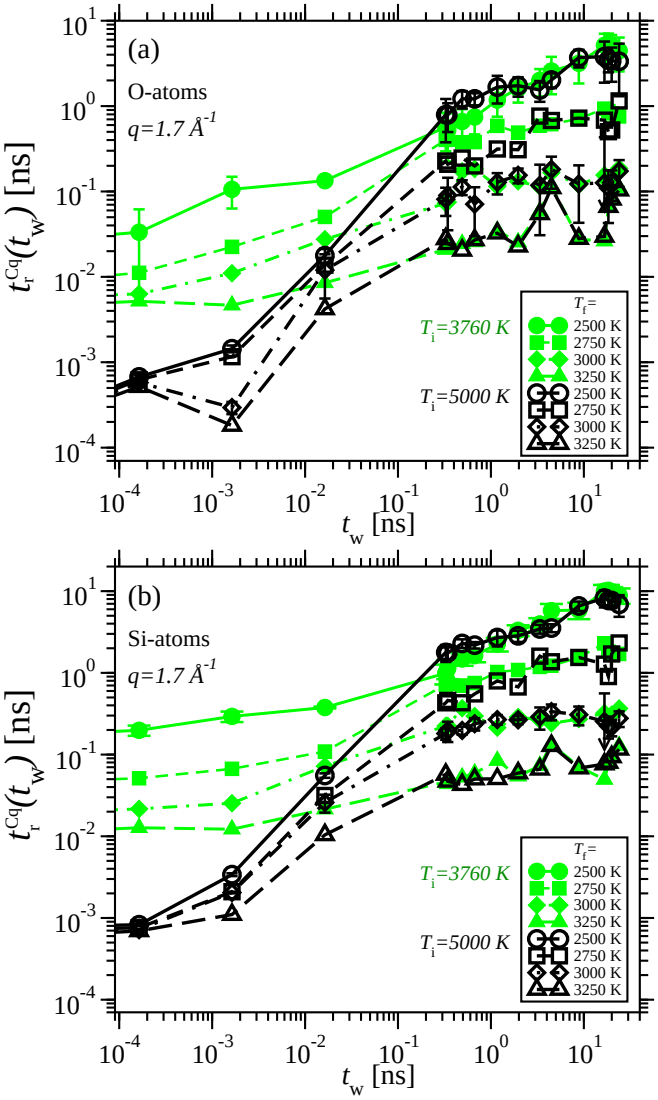

FIG. 7: (Color online) Decay time t_r^Cq for $q = 1.7$ Å^{-1} and (a) O-atoms and (b) Si-atoms. Green (gray) is used for $T_\mathrm{i} = 3760$ K and black for $T_\mathrm{i} = 5000$ K. Symbol shape indicates T_f as given in the legend. Error bars are given exemplary for ($T_\mathrm{i} = 3760$ K, $T_\mathrm{f} = 2500$ K), ($T_\mathrm{i} = 5000$ K, $T_\mathrm{f} = 2500$ K) and ($T_\mathrm{i} = 5000$ K, $T_\mathrm{f} = 3000$ K).

and symbol shape indicates the final temperature T_f.

We find that $t_\mathrm{r}^\mathrm{Cq}(t_\mathrm{w})$ is characterized by three different t_w-windows. (I) For waiting times $t_\mathrm{w} \lesssim 0.3$ ns, decay times are significantly lower for $T_\mathrm{i} = 5000$ K (black lines and symbols) than for $T_\mathrm{i} = 3760$ K (green/gray lines and symbols). The dependence of t_r^Cq on t_w is strongly dependent on all varied parameters, i.e. T_i, T_f, particle type, and q. For $T_\mathrm{i} = 5000$ K, $T_\mathrm{f} = 2500$ K, 2750 K, and $q = 1.7$ Å^{-1}, 2.7 Å^{-1} $t_\mathrm{r}^\mathrm{Cq}(t_\mathrm{w})$ follows roughly a power law with an exponent $\mu \approx 1.15$ with variations of the order of 0.07 dependent on T_f, particle type, and q. (II) For intermediate waiting times, $t_\mathrm{r}^\mathrm{Cq}(t_\mathrm{w})$ also follows roughly a power law with a different exponent than in regime (I). We find for $T_\mathrm{i} = 5000$ K, $T_\mathrm{f} = 2500$ K, 2750 K and $q = 1.7$ Å^{-1}, 2.7 Å^{-1} $\mu \approx 0.35$ with variations of the order of 0.08 depending on T_f, particle type, and q. Best power law fits are for $T_\mathrm{i} = 3760$ K, $T_\mathrm{f} = 2500$ K with μ ranging from $\mu = 0.55/0.57$ for $q = 1.7$ Å^{-1} to $\mu = 0.69/0.63$ for $q = 6.6$ Å^{-1} and for Si/O atoms. Kob and Barrat find for the binary Lennard-Jones system also a power law for $t_\mathrm{r}^\mathrm{Cq}(t_\mathrm{w})$, however, with $\mu = 0.882$ [16]. Similar to Grigera et al. [47] we find that the transition from small

waiting times (I) to intermediate waiting times (II) is accompanied by a change of the exponent μ. (III) For very long waiting times $t_{\rm r}^{\rm Cq}(t_{\rm w})$ is independent of $t_{\rm w}$ and $T_{\rm i}$, i.e. equilibrium is reached. The waiting time t_{23} for which the transition from regime (II) to regime (III) occurs is dependent on $T_{\rm f}$: $t_{23} \approx 0.3\,{\rm ns}$ for $T_{\rm f} = 3250\,{\rm K}$, $t_{23} \approx 1\,{\rm ns}$ for $T_{\rm f} = 3000\,{\rm K}$, $t_{23} \approx 3\,{\rm ns}$ for $T_{\rm f} = 2750\,{\rm K}$, and $t_{23} \approx 10\,{\rm ns}$ for $T_{\rm f} = 2500\,{\rm K}$.[54]

Mean-field spin glass models predict [8, 9]

$$C_q(t_{\rm w}, t_{\rm w}+t) = C_q^{\rm ST}(t) + C_q^{\rm AG}\left(\frac{h(t_{\rm w}+t)}{h(t_{\rm w})}\right), \quad (4)$$

according to which $C_q(t_{\rm w}, t_{\rm w}+t)$ can be separated into a short-time term $C_q^{\rm ST}(t)$ that is independent of t_w and an intermediate-time term that scales as $h(t_{\rm w}+t)/h(t_{\rm w})$ where h is a monotonously increasing function. It has been observed for different systems that the function $h(t)$ follows $h(t) \approx t^{\alpha}$. Thus, the so-called "simple aging" (see [16] and references therein) applies and, as a consequence, C_q as a function of $(t/t_{\rm w})$ for different $t_{\rm w}$ superimpose.

Müssel and Rieger [48] have proposed activated dynamics for $C_q(t_{\rm w}, t_{\rm w}+t)$,

$$C_q(t_{\rm w}, t_{\rm w}+t) = C_q^{\rm ST}(t) + C_q^{\rm AG}\left(\frac{\ln\left[(t_{\rm w}+t)/\tau_{\rm fit}\right]}{\ln\left[t_{\rm w}/\tau_{\rm fit}\right]}\right), \quad (5)$$

where the characteristic time scale $\tau_{\rm fit}$ is a fit parameter. We find that neither $C_q\left(\frac{t_{\rm w}+t}{t_{\rm w}}\right)$, nor $C_q\left(\frac{t}{t_{\rm w}}\right)$, nor $C_q\left(\frac{\ln[(t_{\rm w}+t)/\tau_{\rm fit}]}{\ln[t_{\rm w}/\tau_{\rm fit}]}\right)$ (for any choice of $\tau_{\rm fit}$) superimpose for different $t_{\rm w}$. Instead we find, similar to the results of Kob and Barrat [16] for a binary Lennard-Jones system, that time superposition holds, defined by

$$C_q(t_{\rm w}, t_{\rm w}+t) = C_q^{\rm ST}(t) + C_q^{\rm AG}\left(\frac{t}{t_{\rm r}^{\rm Cq}(t_{\rm w})}\right). \quad (6)$$

In Fig. 8, we show $C_q(t/t_{\rm r}^{\rm Cq})$ for the same set of parameters as in Fig. 4. When all waiting times are included (see inset of Fig. 8) time superposition does not apply due to including too short waiting times. Wahlen and Rieger [26] have studied $C_q(t_{\rm w}, t_{\rm w}+t)$ for the same BKS-SiO_2 system, however for waiting times smaller than 50 ps. Their results are consistent with the inset of Fig. 8. For waiting times $t_{\rm w} \geq 0.49\,{\rm ns}$ (see Fig. 8), however, Eq. (6) is a good approximation. Please note that $C_q(t/t_{\rm r}^{\rm Cq})$ follows time superposition for all waiting times $t_{\rm w} \geq 0.49\,{\rm ns}$, i.e. not only for the time-range (II), but also for the time-range (III). That means for the α-relaxation that the shape of the out-of equilibrium curves is the same (within error bars) as the shape of the equilibrium curves. We find similar results for all other $(T_{\rm i}, T_{\rm f})$ combinations, Si-particles, and all other q.

Next we test whether $C_q = C(q, t_{\rm w}, t_{\rm w}+t)$ scales as $C_q = C(q, z(t_{\rm w}, t)$ where z is a function of $t_{\rm w}$ and t only, i.e. independent of q. Following an approach of Kob and Barrat [17] we show in Figure 9 a parametric plot for

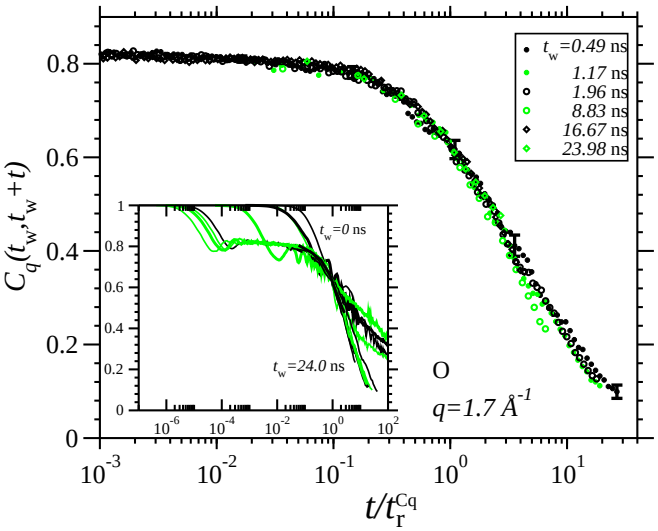

FIG. 8: (Color online) $C_q(t/t_{\rm r}^{\rm Cq})$ for the quench from $T_{\rm i} = 2500\,{\rm K}$ to $T_{\rm i} = 5000\,{\rm K}$ for O-atoms and $q = 1.7\,{\rm Å}^{-1}$. Waiting times and corresponding lines in the inset are the same as in Fig. 4.

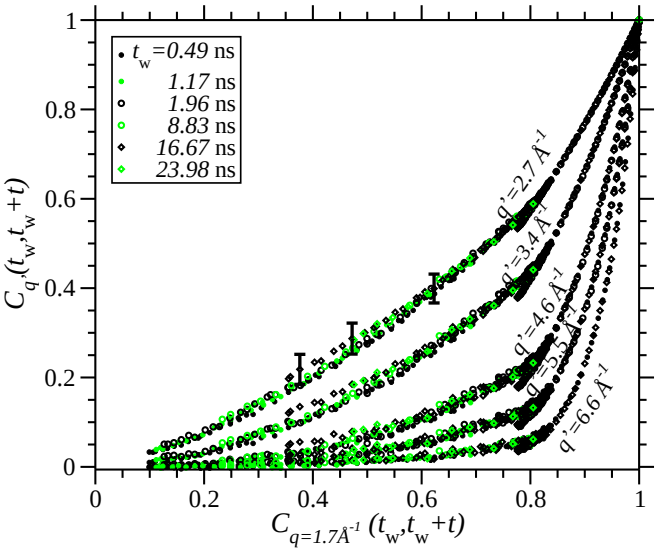

FIG. 9: (Color online) $C_{q'}(t_{\rm w}, t_{\rm w}+t)$ as a function of $C_q(t_{\rm w}, t_{\rm w}+t)$ for $q = 1.7\,{\rm Å}^{-1}$ and $q' = 2.7$, 3.4, 4.6, 5.5, $6.6\,{\rm Å}^{-1}$ for O-atoms and the temperature quench from 5000 K to 2500 K.

$C_{q'}(t_{\rm w}, t_{\rm w}+t)$ as a function of $C_q(t_{\rm w}, t_{\rm w}+t)$ for $q = 1.7\,{\rm Å}^{-1}$ and $q' = 2.7$, 3.4, 4.6, 5.5, $6.6\,{\rm Å}^{-1}$ for O-atoms and the temperature quench from 5000 K to 2500 K. For sufficiently large $t_{\rm w}$ we find, contrary to the results of Kob and Barrat for the Lennard-Jones system, that for SiO_2 the parametric curves superimpose and thus that $C(q, t_{\rm w}, t_{\rm w}+t) = C(q, z(t_{\rm w}, t)$ for $t_{\rm w} \geq 0.49$ ns. This includes, within error bars, also the equilibrated curves for $t_{\rm w} \gtrsim 10\,{\rm ns}$. We find similar results for all other $(T_{\rm i}, T_{\rm f})$ combinations, Si-particles, and all other q.

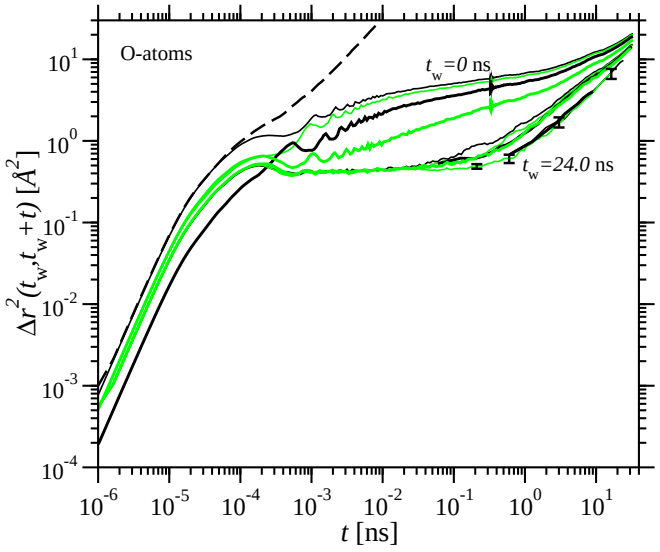

FIG. 10: (Color online) Mean square displacement $\Delta r^2(t_\mathrm{w}, t_\mathrm{w}+t)$ as defined in Eq. (7) for the temperature quench from 5000 K to 2500 K and for O-atoms. Waiting times and corresponding line styles are the same as in Fig. 4.

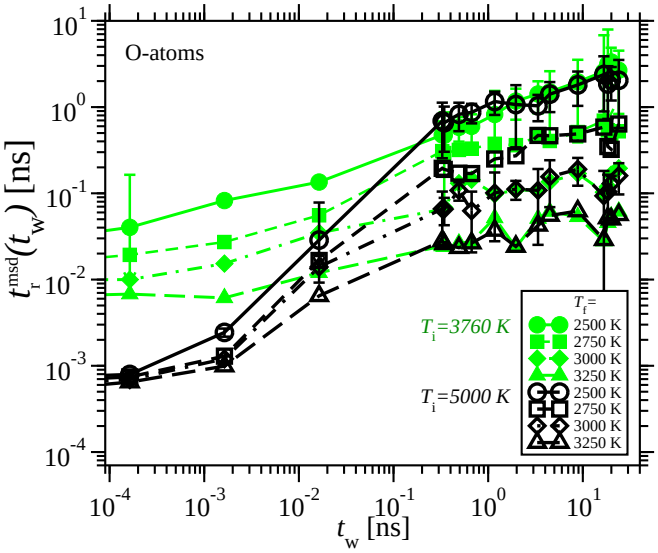

FIG. 11: (Color online) $t_\mathrm{r}^\mathrm{msd}$ for O-atoms. Symbols for the different $(T_\mathrm{i}, T_\mathrm{f})$ combinations are the same as in Fig. 7. Error bars are indicated exemplary for (3760 K, 2500 K), (5000 K, 2500 K) and (5000 K, 3000 K).

C. Mean Square Displacement

In the previous section, we have focused on the analysis of $C_q(t_\mathrm{w}, t_\mathrm{w}+t)$ and identified different time-windows. In this section, we consider the mean square displacement

$$\Delta r^2(t_\mathrm{w}, t_\mathrm{w}+t) = \frac{1}{N}\sum_{i=1}^{N}\left\langle \left(\mathbf{r}_i(t_\mathrm{w}+t) - \mathbf{r}_i(t_\mathrm{w})\right)^2 \right\rangle . \quad (7)$$

Figure 10 shows $\Delta r^2(t_\mathrm{w}, t_\mathrm{w}+t)$ for the temperature quench from 5000 K to 2500 K and for O-atoms. As in Fig. 4, for times $t \lesssim 5\cdot 10^{-5}$ ns and zero waiting time, the mean square displacement $\Delta r^2(t_\mathrm{w}=0, t)$ is well approximated by Δr^2 of the high temperature $T_\mathrm{i} = 5000$ K from which the system has been quenched (see dashed line in Fig. 10) and thus independent of T_f. For times $t \approx 10^{-3}$ ns, $\Delta r^2(t_\mathrm{w}, t_\mathrm{w}+t)$ is oscillatory due to the small system size [31], while for times $t \gtrsim 10^{-3}$ ns and waiting times $t_\mathrm{w} \geq 0.33$ ns, we find that Δr^2 forms a plateau which is independent of t_w. As for C_q, we find that the plateau is the more horizontal the smaller T_f and the plateau height depends on the particle type but is independent of T_i.

For waiting times $t_\mathrm{w} \geq 0.33$ ns and times $t \gtrsim 0.1$ ns, the mean square displacement leaves the plateau and increases further. To characterize the dependence of this α-relaxation we define the time $t_\mathrm{r}^\mathrm{msd}$ as the time $t = t_\mathrm{r}^\mathrm{msd}$ for which $\Delta r^2(t_\mathrm{w}, t_\mathrm{w}+t_\mathrm{r}^\mathrm{msd}) = 1.35$ Å^2 (see Fig. 11). We can identify again the three time windows (I) of waiting times $t_\mathrm{w} \lesssim 0.3$ ns with a dependence on T_i, T_f and particle type, (II) the aging regime of intermediate waiting times where $t_\mathrm{r}^\mathrm{msd}$ follows roughly a power law, and (III) for very long waiting times when equilibrium is reached. The transition from (II) to (III) occurs at approximately the same times t_{23} as for C_q, i.e. $t_{23} \approx 0.3$ ns for $T_\mathrm{f} = 3250$ K, $t_{23} \approx 1$ ns for $T_\mathrm{f} = 3000$ K, $t_{23} \approx 3$ ns for $T_\mathrm{f} = 2750$ K and $t_{23} \approx 10$ ns for $T_\mathrm{f} = 2500$ K.

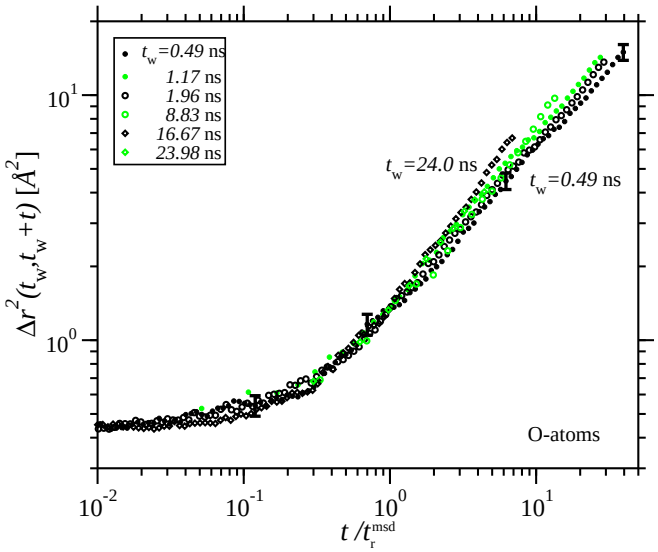

FIG. 12: (Color online) $\Delta r^2(t/t_\mathrm{r}^\mathrm{msd})$ for the temperature quench from 5000 K to 2500 K and for O-atoms.

Figure 12 shows the equivalent of Fig. 8 to test time superposition. We find for $\Delta r^2(t/t_\mathrm{r}^\mathrm{msd})$ that time superposition is valid for waiting times 0.34 ns $\leq t_\mathrm{w} \lesssim$ 8.83 ns, i.e. for the time window (II) but not for the time window (III).

IV. SUMMARY

Using molecular dynamics simulations, we investigated for the strong glass former SiO_2 the aging dynamics below the critical MCT temperature T_c, using the BKS potential to model the interactions between silicon and oxygen atoms. After an instantaneous quench from $T_\mathrm{i} > T_c$ to a temperature $T_\mathrm{f} < T_c$ the dynamics towards equilibrium was studied as a function of waiting time t_w. Note that the temperatures T_f were chosen such that equilibrium was reached on the time span of the simulations (of the order of 30 ns). The central quantities considered in this work are the incoherent intermediate scattering function $C_q(t_\mathrm{w}, t_\mathrm{w}+t)$ and the mean square displacement $\Delta r^2(t_\mathrm{w}, t_\mathrm{w}+t)$. These functions depend on the time origin at t_w as long as t_w is smaller than the typical relaxation time, τ_eq, that is required to equilibrate the system.

We find that the decay of $C_q(t_\mathrm{w}, t_\mathrm{w}+t)$ (and similarly the rise of $\Delta r^2(t_\mathrm{w}, t_\mathrm{w}+t)$) exhibit qualitative changes from short to long waiting times. At short waiting times, relaxation processes are dominant that correspond to the early β relaxation regime at the target temperature T_f. In this t_w regime, no well-defined plateau is found in $C_q(t_\mathrm{w}, t_\mathrm{w}+t)$ (see Fig. 4). Instead, this function first decreases rapidly, followed by a strongly stretched exponential decay to zero. At long waiting times, the β relaxation seems to be very similar to that at equilibrium. The Debye-Waller factor (i.e. the height of the plateau in $C_q(t_\mathrm{w}, t_\mathrm{w}+t)$) has reached its equilibrium value, although the decay of $C_q(t_\mathrm{w}, t_\mathrm{w}+t)$ from the plateau to zero is faster than that at equilibrium. However, the shape of curves describing the long-time decay of $C_q(t_\mathrm{w}, t_\mathrm{w}+t)$ is the same as that at equilibrium. Thus, C_q follows a simple time superposition for long waiting times, different e.g. from the "activated dynamics scaling" proposed by Wahlen and Rieger for BKS silica.

Our results show that the aging dynamics of BKS silica is very similar to that of the KALJ mixture. For both silica and the KALJ mixture three t_w-regimes can be identified and C_q follows time superposition for sufficiently large t_w. The only difference between these two systems is that C_q scales as $C(q, z(t_\mathrm{w}, t)$ for SiO_2 but less well for the KALJ mixture. So slightly below its critical temperature T_c of MCT, the strong glass-former silica does not seem to be very different from typical fragile systems, although one has already reached the low temperature Arrhenius regime (note that activation energies for the self-diffusion, viscosity etc. are of the order of 5 eV, similar to the corresponding activation energies close to the glass transition temperature $T_\mathrm{g} \approx 1450\,\mathrm{K}$, as measured in various experiments). However, the dynamics could be very different at very low temperatures (close to T_g) where the long-time aging regime is not accessible by computer simulations. Thus, more experimental work on the aging dynamics of silica around T_g would be very desirable. We also leave for future work to test whether also for other systems three t_w-regimes are identified and whether the equilibrium curve is included in the time superposition of C_q at intermediate and large t_w.

Acknowledgments

KVL thanks A. Zippelius and the Institute of Theoretical Physics, University of Göttingen, for hospitality and financial support.

Appendix A: Velocity Verlet Nosé Hoover

The Nosé Hoover equations of motion are for particles $i = 1, \ldots, N$ at position $\mathbf{r_i}$ with momentum $\mathbf{p_i}$

$$\dot{\mathbf{r}}_i = \frac{\mathbf{p}_i}{m_i} \tag{A1}$$

$$\dot{\mathbf{p}}_i = \mathbf{F}_i - \zeta \mathbf{p}_i \tag{A2}$$

$$\dot{\zeta} = \frac{1}{Q}\left(\sum_{i=1}^{N} \frac{\mathbf{p}_i^2}{m_i} - XkT\right) \tag{A3}$$

and thus

$$\ddot{\mathbf{r}}_i = \frac{\mathbf{F}_i}{m_i} - \zeta\, \dot{\mathbf{r}}_i \tag{A4}$$

$$\frac{\mathrm{d}^2 \ln s}{\mathrm{d}t^2} = \dot{\zeta} = \frac{1}{Q}\left(\sum_{i=1}^{N} m_i \dot{\mathbf{r}}_i^2 - XkT\right) \tag{A5}$$

where $X = 3N$. We integrated with the generalized velocity Verlet form of Fox and Andersen [49]

$$\mathbf{r}_i(t+\Delta t) = \mathbf{r}_i(t) + \Delta t\, \dot{\mathbf{r}}_i(t) + \frac{(\Delta t)^2}{2}\left(\frac{\mathbf{F}_i(t)}{m_i} - \zeta(t)\, \dot{\mathbf{r}}_i(t)\right) \tag{A6}$$

$$\ln s(t+\Delta t) = \ln s(t) + \Delta t\, \zeta(t) + \frac{(\Delta t)^2}{2Q}\left(\sum_{i=1}^{N} m_i \dot{\mathbf{r}}_i^2(t) - XkT\right) \tag{A7}$$

$$\zeta^{\mathrm{approx}}(t+\Delta t) = \zeta(t) + \frac{\Delta t}{Q}\left(\sum_{i=1}^{N} m_i \dot{\mathbf{r}}_i^2(t) - XkT\right) \tag{A8}$$

$$\dot{\mathbf{r}}_i(t+\Delta t) = \dot{\mathbf{r}}_i(t) + \frac{\Delta t}{2}\Bigg(\frac{\mathbf{F}_i(t) + \mathbf{F}_i(t+\Delta t)}{m_i} - \big[\zeta(t) + \zeta^{\mathrm{approx}}(t+\Delta t)\big]\dot{\mathbf{r}}_i(t)\Bigg) \Bigg(1 - \frac{\Delta t}{2}\zeta^{\mathrm{approx}}(t+\Delta t)\Bigg) \tag{A9}$$

$$\zeta(t+\Delta t) = \zeta(t) + \frac{\Delta t}{2Q}\Big(\sum_{i=1}^{N} m_i \dot{\mathbf{r}}_i^2(t) + \sum_{i=1}^{N} m_i \dot{\mathbf{r}}_i^2(t+\Delta t) - 2XkT\Big) \tag{A10}$$

To ensure that $\Upsilon = \sum_{i=1}^{N} \frac{\mathbf{p}_i^2}{2m_i} + U(\{\mathbf{r}_i\}) + \frac{Q}{2}\zeta^2 + XkT\ln s$ is conserved (see [46]) we chose $Q = 50000$ Å^2 u.

[1] L. Cipelletti and L. Ramos, J. Phys.: Condens. Matter **17**, R253 (2005).
[2] J. M. Lynch, G. C. Cianci, and E. R. Weeks, Phys. Rev. E **78**, 031410 (2008).
[3] G. C. Cianci, R. E. Courtland, and E. R. Weeks, Solid State Commun. **139**, 599 (2006).
[4] R. E. Courtland and E. R. Weeks, J. Phys.: Condens. Matter **15**, S359 (2003).
[5] K. N. Pham, S. U. Egelhaaf, P. N. Pusey, and W. C. K. Poon, Phys. Rev. E **69**, 011503 (2004).
[6] A. Latka, Y. Han, A. M. Alsayed, A. B. Schofield, A. G. Yodh, and P. Habdas, Europhys. Lett. **86**, 58001 (2009).
[7] L. F. Cugliandolo and J. Kurchan, Phys. Rev. Lett. **71**, 173 (1993).
[8] J.-P. Bouchaud, L. F. Cugliandolo, J. Kurchan, and M. Mèzard, Physica A **226**, 243 (1996).
[9] J.-P. Bouchaud, L. F. Cugliandolo, M. Mèzard, and J. Kurchan, arXiv.org **arXiv:cond-mat/9702070v1 [cond-mat.dis-nn]** (1997).
[10] J.-L. Barrat, M. Feigelman, J. Kurchan, and J. Dalibard, eds., *Slow Relaxations and Nonequilibrium Dynamics in Condensed Matter* (Springer, 2003).
[11] K. Binder and W. Kob, *Glassy Materials and Disordered Solids – An Introduction to Their Statistical Mechanics* (World Scientific, London, 2005).
[12] G. Foffi, E. Zaccarelli, S. Buldyrev, F. Sciortino, and P. Tartaglia, J. Chem. Phys. **120**, 8824 (2004).
[13] G. Foffi, C. DeMichele, F. Sciortino, and P. Tartaglia, Phys. Rev. Lett. **94**, 078301 (2005).
[14] G. Foffi, C. D. Michele, F. Sciortino, and P. Tartaglia, J. Chem. Phys. **122**, 224903 (2005).
[15] A. M. Puertas, M. Fuchs, and M. E. Cates, Phys. Rev. E **75**, 031401 (2007).
[16] W. Kob and J.-L. Barrat, Phys. Rev. Lett. **78**, 4581 (1997).
[17] W. Kob and J.-L. Barrat, Eur. Phys. J. B **13**, 319 (2000).
[18] J.-L. Barrat and W. Kob, Europhys. Lett. **46**, 637 (1999).
[19] W. Kob, F. Sciortino, and P. Tartaglia, Europhys. Lett. **49**, 590 (2000).
[20] F. Sciortino and P. Tartaglia, J. Phys.: Condens. Matter **13**, 9127 (2001).
[21] I. Saika-Voivod and F. Sciortino, Phys. Rev. E **70**, 041202 (2004).
[22] A. Parsaeian and H. E. Castillo, Phys. Rev. E **78**, 060105(R) (2008).
[23] A. Parsaeian and H. E. Castillo, Phys. Rev. Lett. **102**, 055704 (2009).
[24] S. Mossa, G. Ruocco, F. Sciortino, and P. Tartaglia, Philos. Mag. B **82**, 695 (2002).
[25] L. Berthier, Phys. Rev. Lett. **98**, 220601 (2007).
[26] H. Wahlen and H. Rieger, J. Phys. Soc. Japan Suppl. A **69**, 242 (2000).
[27] A. Scala, C. Valeriani, F. Sciortino, and P. Tartaglia, Phys. Rev. Lett. **90**, 115503 (2003).
[28] A. Parsaeian, H. E. Castillo, and K. Vollmayr-Lee, to be published.
[29] K. Vollmayr, W. Kob, and K. Binder, Phys. Rev. B **54**, 15808 (1996).
[30] J. Horbach and W. Kob, Phys. Rev. B **60**, 3169 (1999).
[31] J. Horbach, W. Kob, K. Binder, and C. A. Angell, Phys. Rev. E **54**, R5897 (1996).
[32] R. L. C. Vink and G. T. Barkema, Phys. Rev. B **67**, 245201 (2003).
[33] I. Saika-Voivod, P. H. Poole, and F. Sciortino, Nature **412**, 514 (2001).
[34] I. Saika-Voivod, F. Sciortino, T. Grande, and P. H. Poole, Phys. Rev. E **70**, 061507 (2004).
[35] A. Saksaengwijit, J. Reinisch, and A. Heuer, Phys. Rev. Lett. **93**, 235701 (2004).
[36] J. Reinisch and A. Heuer, Phys. Rev. Lett. **95**, 155502 (2005).
[37] A. Saksaengwijit and A. Heuer, Phys. Rev. E **73**, 061503 (2006).
[38] A. Saksaengwijit and A. Heuer, J. Phys.: Condens. Matter **19**, 205143 (2007).
[39] P. Scheidler, W. Kob, A. Latz, J. Horbach, and K. Binder, Phys. Rev. B **63**, 104204 (2001).
[40] B. W. H. van Beest, G. J. Kramer, and R. A. van Santen, Phys. Rev. Lett. **64**, 1955 (1990).
[41] J. Kieffer and C. A. Angell, J. Chem. Phys. **90**, 4982 (1989).
[42] M. P. Allen and D. J. Tildesley, *Computer Simulation of Liquids* (Oxford University Press, New York, 1990).
[43] P. Pfleiderer, J. Horbach, and K. Binder, Chem. Geol. **229**, 186 (2006).
[44] R. Brückner, J. Non-Cryst. Solids **5**, 123 (1970).
[45] W. G. Hoover, Phys. Rev. A **31**, 1695 (1985).
[46] A. C. Brańka and K. W. Wojciechowski, Phys. Rev. E **62**, 3281 (2000).
[47] T. S. Grigera, V. Martín-Mayor, G. Parisi, and P. Verrocchio, Phys. Rev. B **70**, 014202 (2004).
[48] U. Müssel and H. Rieger, Phys. Rev. Lett. **81**, 930 (1998).
[49] J. R. Fox and H. C. Andersen, J. Phys. Chem. **88**, 4019 (1984).
[50] M. Abramovitz and I. A. Stegun, *Handbook of Mathematical Functions* (Dover Publications, New York, 1972).
[51] The erfc was approximated with a polynomial of fifth order [50].
[52] Please note that we chose all parameters as described in [43] with the only exception of $a_{2,\mathrm{O}} = 895.11679$ eV/Å(instead of $a_{2,\mathrm{O}} = 90.38499$ eV/Å).
[53] Both the duration of the NVT-simulation run, as well as the Nosé-Hoover parameter Q were chosen carefully such that Υ and E_{tot} were constant during the NVT and NVE runs respectively.
[54] These estimates of t_{23} are in good agreement with the results of Scheidler et al. [39] who determined the relaxation time via the specific heat and who found good agreement with experimental data.